

Supplementary Information

Dopant site in indium-doped SrTiO₃ photocatalysts

Hanggara Sudrajat,* Mohamed M. Fadlallah, Shuxia Tao, Mitsunori Kitta, Nobuyuki Ichikuni, and Hiroshi Onishi

Corresponding Author

Hanggara Sudrajat – *Department of Chemistry, Graduate School of Science, Kobe University, Kobe 657-8501, Japan*

– *Department of Chemical Engineering, Faculty of Engineering, Universitas Jember, Jember 68121, Indonesia*; ORCID ID: 0000-0002-1775-3127; Email: hanggara@unej.ac.id

Authors

Mohamed M. Fadlallah – *Center for Computational Energy Research, Department of Applied Physics, Eindhoven University of Technology, Eindhoven 5600, the Netherlands*
- *Department of Physics, Faculty of Science, Benha University, Benha 13518, Egypt*, ORCID ID: 0000-0003-2102-1022.

Shuxia Tao – *Center for Computational Energy Research, Department of Applied Physics, Eindhoven University of Technology, Eindhoven 5600, the Netherlands*. ORCID ID: 0000-0002-3658-8497

Mitsunori Kitta – *Research Institute of Electrochemical Energy, Department of Energy and Environment, National Institute of Advanced Industrial Science and Technology, Osaka 563-8577, Japan*; ORCID ID: 0000-0001-9800-7371

Nobuyuki Ichikuni – *Department of Applied Chemistry and Biotechnology, Graduate School of Engineering, Chiba University, Chiba 263-8522, Japan*; ORCID ID: 0000-0002-4241-061X

Hiroshi Onishi – *Department of Chemistry, Graduate School of Science, Kobe University, Kobe 657-8501, Japan*; ORCID ID: 0000-0003-1873-9105

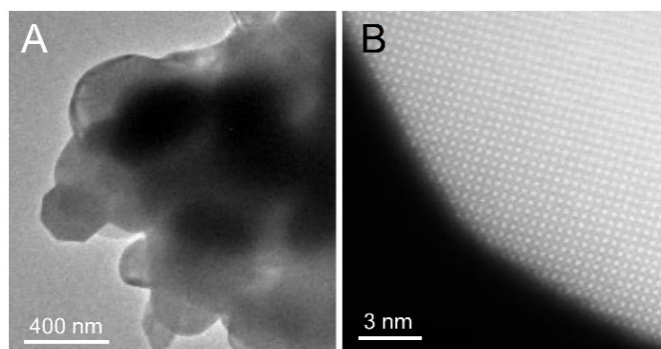


Figure S1. (A) Scanning transmission electron micrograph and (B) annular dark field image of In-STO (7.1 mol%) with Sr atom columns.

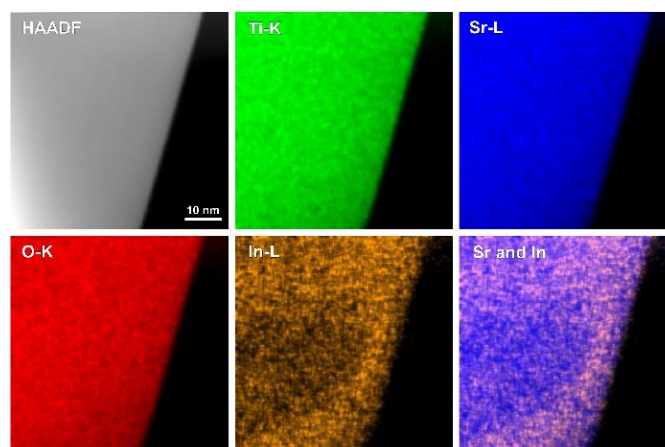


Figure S2. High-resolution annular dark field image of In-STO (7.1 mol%) with element maps.

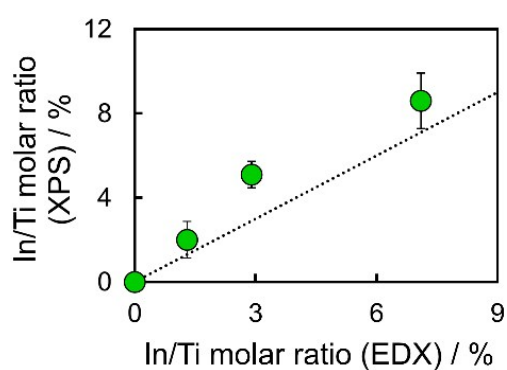


Figure S3. Surface In concentration (determined by XPS) with error bars as a function of the bulk In concentration (determined by EDX). The broken line denotes the relationship with a slope of 1.

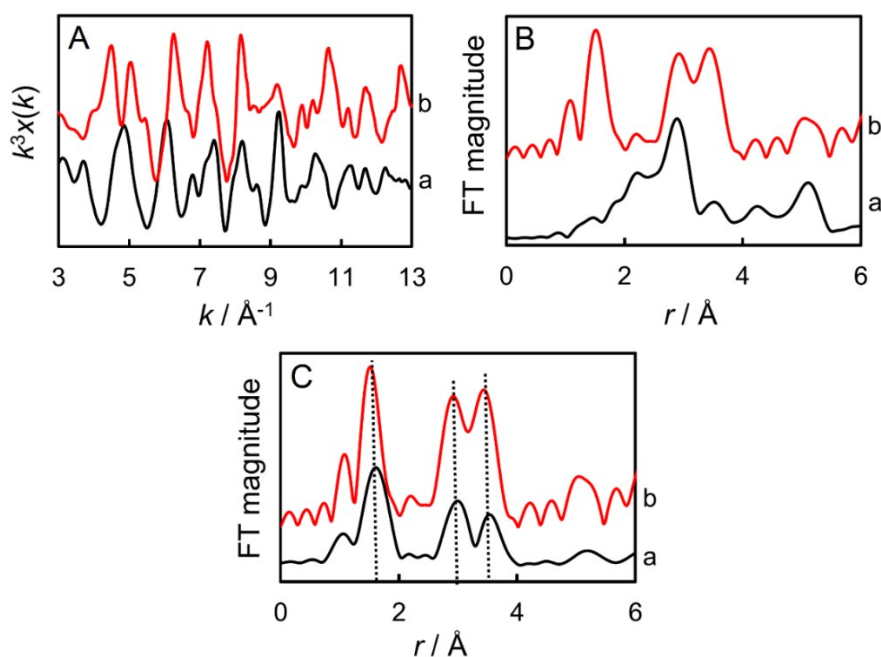


Figure S4. (A) The k^3 -weighted absorption spectra and (B) radial distribution functions of SrTiO₃ at (a) the Sr *K*-edge and (b) the Ti *K*-edge. (C) Radial distribution functions (a) at the In *K*-edge of SrTiO₃ doped with 1.3 mol% of In and (b) at the Ti *K*-edge of SrTiO₃.

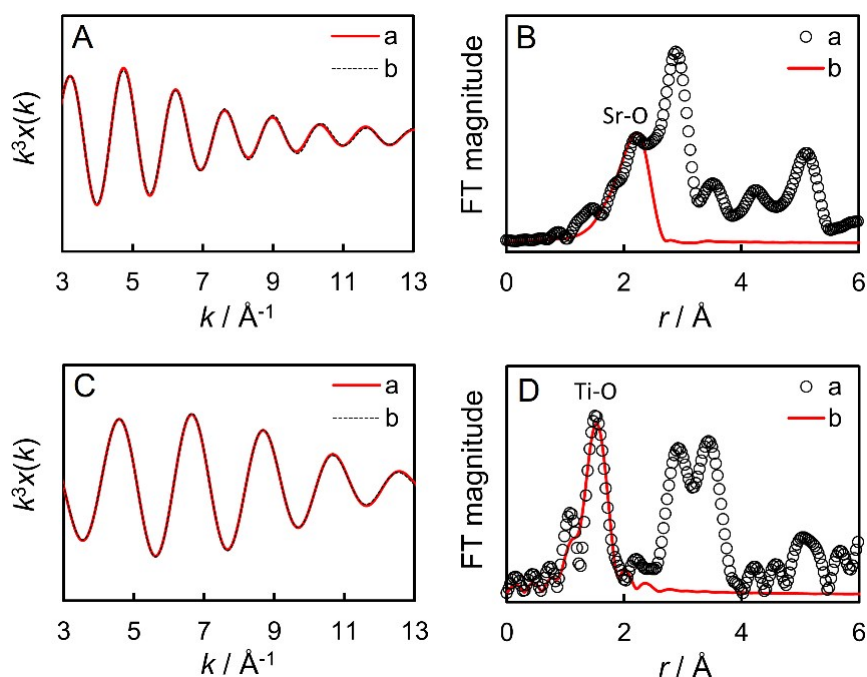


Figure S5. (a) Fourier-filtered and (b) fitted k^3 -weighted absorption spectra of SrTiO₃ at (A) the Sr *K*-edge for the Sr-O coordination and (C) the Ti *K*-edge for the Ti-O coordination. (a) Observed and (b) fitted radial distribution functions of SrTiO₃ at (B) the Sr *K*-edge for the Sr-O coordination and (D) the Ti *K*-edge for the Ti-O coordination.

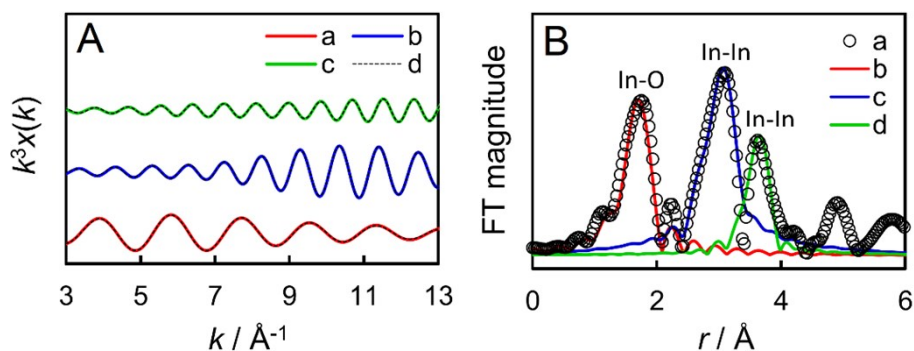


Figure S6. (A) Fourier-filtered (a) In-O, (b) In-In, (c) In-In and (d) fitted k^3 -weighted absorption spectra at the In K -edge of In_2O_3 . (B) (a) Observed and fitted (b) In-O, (c) In-In, (d) In-In radial distribution functions of In_2O_3 .

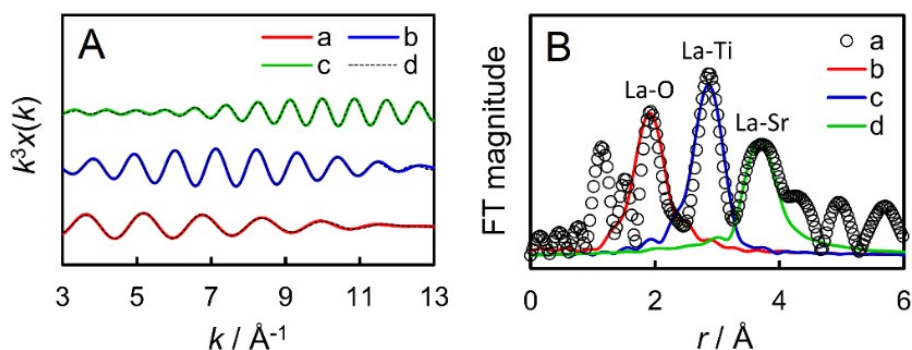


Figure S7. Fourier-filtered (a) La-O, (b) La-Ti, (c) La-Sr and (d) fitted k^3 -weighted absorption spectra at the In K -edge of (A) La-STO (2.8 mol%). (a) Observed and fitted (b) La-O, (c) La-Ti, (d) La-Sr radial distribution functions of (B) La-STO (2.8 mol%).

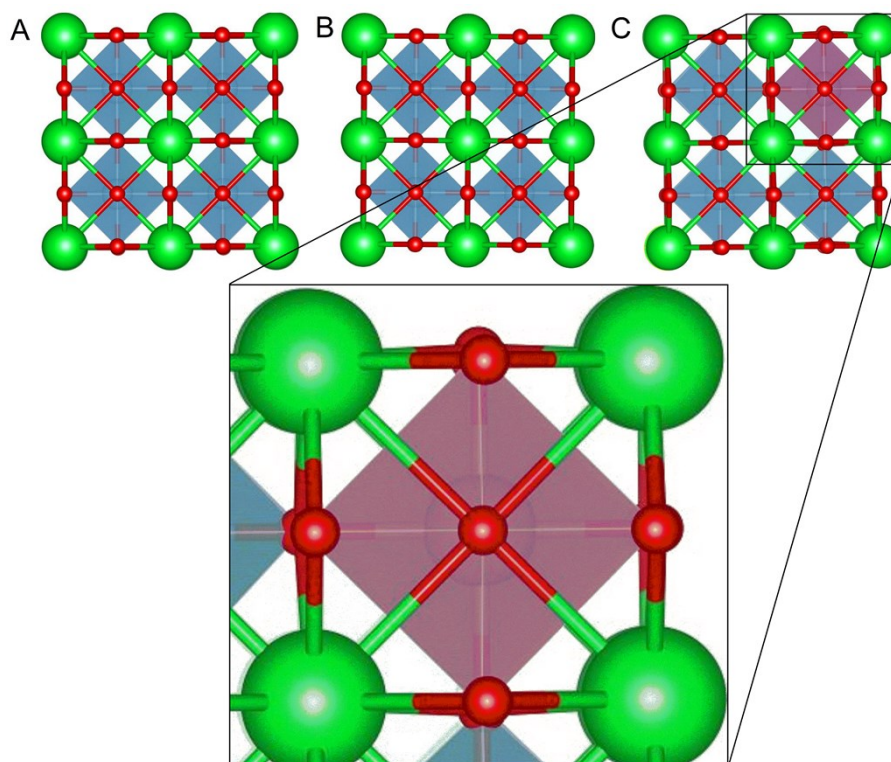


Figure S8. Structurally optimized $2 \times 2 \times 2$ supercells of (A) STO, (B) In(A)-STO, and (C) In(B)-STO viewed from the $\langle 001 \rangle$ zone-axis. A part of the In(B)-STO supercell is enlarged to show the distorted sublattice. The green, blue, red and pink spheres refer to Sr, Ti, O, and In atoms, respectively.